Virology 568 (2022) 126–139

Contents lists available at ScienceDirect

Virology

journal homepage: www.elsevier.com/locate/virology

Subcellular dynamics of red clover necrotic mosaic virus double-stranded RNAs in infected plant cells

Shota Takata [a], Kazuyuki Mise [a], Yoshitaka Takano [a], Masanori Kaido [a,b,*]

[a] Laboratory of Plant Pathology, Graduate School of Agriculture, Kyoto University, Kyoto, 606-8502, Japan
[b] Laboratory of Plant Environmental Microbiology, Department of Applied Biological Sciences, Setsunan University, Hirakata, 573-0101, Japan

ARTICLE INFO

Keywords:
Viral replication complex (VRC)
Movement protein
Positive-strand RNA virus
Dianthovirus
Endoplasmic reticulum

ABSTRACT

New evidences are emerging to support the importance of viral replication complexes (VRCs) in not only viral replication, but also viral cell-to-cell movement. Currently, how VRCs grow in size and colocalize with viral movement proteins (MPs) remains unclear. Herein, we performed live-cell imaging of red clover necrotic mosaic virus (RCNMV) dsRNA by using reporter B2-GFP plants. Tiny granules of dsRNA were formed along the endoplasmic reticulum (ER) at an early stage of infection. Importantly, the colocalization of the dsRNA granules with the virus-encoded p27 replication protein showed that these structures are components of VRCs. These granules moved throughout the cytoplasm, driven by the acto–myosin system, and coalesced with each other to form larger aggregates; the MPs were not associated with these processes. Notably, the MPs colocalized preferentially with large dsRNA aggregates, rather than with tiny dsRNA granules, suggesting that the increase in the size of VRCs promotes their colocalization with MPs.

1. Introduction

Most positive-strand RNA viruses modify the membrane structure of cellular organelles, such as the endoplasmic reticulum (ER), peroxisomes, and Golgi apparatus, to form viral replication complexes (VRCs) and synthesize viral RNA (den Boon et al., 2010; Heinlein et al., 1998; Laliberté and Sanfaçon, 2010; Laliberté and Zheng, 2014; Mine and Okuno, 2012). As viruses encode only a few proteins, they must utilize several host proteins to form a suitable microenvironment for replication (Hyodo and Okuno, 2014, 2016, 2020; Nagy and Feng, 2021). VRCs contain viral replicase, genomic RNA, double-stranded RNA (dsRNA), an intermediate product of viral replication, and host proteins. Replicase alters the membrane structure of the host cell organelle, resulting in the reorganization of the endomembrane upon VRC formation (den Boon and Ahlquist, 2010). Electron microscopy analysis of yeast cells expressing the 1a protein, a replicase component of brome mosaic virus, showed the formation of spherules about 50 nm in diameter that contain the viral replicase proteins (Schwartz et al., 2002). The formation of spherules involves endosomal sorting complexes required for transport (ESCRT) and the reticulon, which functions during ER remodeling-associated processes, such as membrane detachment and bending (Diaz et al., 2010, 2015). These structures are thought to be the sites of viral replication; they protect the viral dsRNA from host RNase (Schwartz et al., 2002, 2004).

VRCs formed by several types of viruses are not static and change their sizes and subcellular localization as the infection progresses. During cowpea mosaic virus (CPMV) infection, CPMV VRCs are distributed as spot-like structures throughout the cytoplasm at an early stage of infection, while larger bodies are formed in the center of cells, often near the nucleus at a late stage of infection (Carette et al., 2002). Tobacco mosaic virus (TMV) viral RNA is recruited to the ER membrane via the 5′ cap structure, and then, the initial VRCs are formed as small granules (Christensen et al., 2009). TMV VRCs move along the microfilaments and accumulate at the junction between the cortical ER–actin network with microtubules; these junctions are called cortical microtubule-associated ER sites (cMERs). The initial VRCs collected in the cMERs are targeted to the plasmodesmata (PD) for viral cell-to-cell movement or form larger aggregates (Sambade et al., 2008). Potato virus X (PVX) induces the formation of ER-derived granular VRCs at an early stage of infection (Bamunusinghe et al., 2009) and forms large aggregates called X-bodies or inclusion bodies at a late stage of infection (Linnik et al., 2013; Tilsner et al., 2012). Aggregates formed during the

* Corresponding author. at: Laboratory of Plant Environmental Microbiology, Department of Applied Biological Sciences, Setsunan University, Hirakata, 573-0101, Japan.
E-mail address: masanori.kaido@setsunan.ac.jp (M. Kaido).

https://doi.org/10.1016/j.virol.2022.01.015
Received 20 September 2021; Received in revised form 23 January 2022; Accepted 29 January 2022
Available online 7 February 2022

late stage are believed to be the sites for enhancing the efficiency of viral replication and virion formation via the sequestration of various host proteins and the cytoskeleton. Thus, the transition of VRCs from smaller granular structures to the larger aggregates represents a widely conserved feature of plant virus infection. However, the process of VRC formation and the transition from the smaller VRCs to the larger aggregates remain poorly understood.

Plant viruses move via the PD to adjacent cells (Lucas, 2006; Reagan and Burch-Smith, 2020; Tilsner et al., 2014; Waigmann et al., 2004). Movement proteins (MPs) function to increase the size exclusion limit of the PD and transfer RNA–MP complexes by binding to viral RNAs (Benitez-Alfonso et al., 2010; Kumar and Dasgupta, 2021; Sambade et al., 2008; Waigmann et al., 2004). Several types of viral MPs colocalize with VRCs. Turnip mosaic virus (TuMV) encodes P3N-PIPO protein as a dedicated MP (Cui et al., 2017; Yang et al., 2021). P3N-PIPO localizes at PD to support the recruitment of cylindrical inclusion (CI) protein to PD and subsequent intercellular trafficking of virion or CP/vRNP. In addition, P3N-PIPO colocalizes with $6K_2$-containing vesicles, which are thought to be components of VRCs. Multipartite interaction between TuMV-encoded proteins, such as $6K_2$, P3, P3N-PIPO, and CI may be involved in transporting $6K_2$-containing vesicles to the entrance of PD, possibly facilitating the cell-to-cell movement of TuMV (Chai et al., 2020; Wang, 2021). Barley stripe mosaic virus (BSMV) encodes three types of MPs (triple gene block (TGB) 1, 2, and 3). TGB2 and TGB3 are recruited by the viral γb protein into chloroplasts, where VRCs are formed, and enhance viral cell-to-cell movement (Jiang et al., 2020). These results suggest that viral replication and cell-to-cell movement are tightly linked and that the colocalization of MPs with VRCs may be necessary for the efficient viral cell-to-cell movement.

Thus far, VRC localization in living cells has been investigated by using fluorescent protein (FP)-tagged viral proteins. As FP-tagged viruses usually have a lower replication capacity than wild type (wt) viruses, it is quite difficult to monitor the dynamics of the VRCs. Recently, Monsion et al. (2018) have developed a transgenic *Nicotiana benthamiana* (B2-GFP plant) expressing the GFP-tagged dsRNA-binding domain of the B2 protein encoded by Flock House virus (B2-GFP). B2-GFP binds to, and detects the localization of, dsRNAs that are more than 80 nucleotides long in living infected cells. Punctate-like dsRNA structures (dsRNA granules) and larger aggregated structures were formed only upon viral infection. The aggregated dsRNA structures colocalized with the viral coat protein (CP), MPs, viral genomic RNA, and viral replicase, suggesting that these structures are components of VRCs. Therefore, B2-GFP plants have the potential to be used for monitoring the dynamics of VRCs in living cells.

Red clover necrotic mosaic virus (RCNMV) is a positive-stranded RNA virus with a bipartite genome; it belongs to the genus *Dianthovirus* in the family *Tombusviridae*. Genomic RNA1 encodes the p27 auxiliary replication protein, p88 RNA-dependent RNA polymerase, and CP (Xiong and Lommel, 1989; Xiong et al., 1993b; Zavriev et al., 1996). RNA2 encodes an MP that is required for viral cell-to-cell movement and belongs to the 30K superfamily (Fujiwara et al., 1993; Xiong et al., 1993a). p27 and p88 localize at the ER (Turner et al., 2004) and form 480-kDa complexes, which are components of VRCs, by binding with several host proteins (Hyodo and Okuno, 2014, 2020). GFP-tagged p27 coexpressed with p88 and RNA2 via agroinfiltration localizes at small punctates along ER filaments. Later, larger aggregates containing the modified ER are formed at the perinuclear region (Kusumanegara et al., 2012), suggesting that the localization and morphology of VRCs change along with RCNMV infection.

Expression of GFP-tagged MPs from the CP-encoding region of RCNMV RNA1 makes it possible to monitor the localization of the MPs in living cells (Tremblay et al., 2005; Kaido et al., 2009). This recombinant system revealed that the MP-GFP localizes at the PD at an early infection stage, and later, forms cortical punctate structures. Eventually, larger aggregates are formed adjacent to the nucleus. Immunostaining analysis showed that the MP-GFP colocalized with p27 and dsRNA, which are components of VRCs (Kaido et al., 2009, 2014). Furthermore, we found that 70 C-terminal amino acids of RCNMV MPs are required for both the localization to cortical punctate structures (that are VRCs) and viral cell-to-cell movement (Kaido et al., 2011). In addition, the search for host factors that facilitate the movement of RCNMV revealed that the glyceraldehyde 3-phosphate dehydrogenase A of *N. benthamiana* (NbGAPDH-A) is involved in viral cell-to-cell movement by influencing the localization of MPs to VRCs (Kaido et al., 2014). These results suggest that RCNMV MPs localize at VRCs via 70 C-terminal amino acids with NbGAPDH-A and that the colocalization of MPs with VRCs is essential for efficient viral cell-to-cell movement. However, fundamental questions regarding how VRCs grow and increase in size, and how and when MPs colocalize with VRCs, remain unanswered.

In this study, we investigated the dynamics of dsRNA structures formed during RCNMV infection in B2-GFP plants to gain insights into the formation and transition processes of VRCs. Upon RCNMV infection, cortical punctate dsRNA granules were formed during an early infection stage; these granules then coalesced with each other to form larger aggregates. The colocalization of dsRNA granules with viral replicase was confirmed, indicating that these dsRNA structures are components of VRCs. Remarkably, large aggregates containing the ER colocalized strongly with MPs, while tiny dsRNA granules were weakly associated with both the membrane and MPs. Herein, we present novel findings stating that VRCs containing dsRNA and granular structures containing MPs are formed separately and that the size of VRCs is relevant to their colocalization with MPs.

2. Materials and methods

2.1. Plasmid construction

Plasmids given the prefix “pBIC” were used for agroinfiltration, and “pUC” were used for *in vitro* transcription. The plasmids pBICp88, pBICRC2 and pUCR1 were described previously (Fig. S1, Takeda et al., 2005).

All plasmids were amplified using *Escherichia coli* DH5α strain. All PCR reactions were performed using KOD One PCR master mix (Toyobo, Osaka, Japan), and all the PCR-amplified regions were verified by sequencing. The primers used in this study are listed in Table S1.

The binary vector pBICP35 (Mori et al., 1991) was digested with ClaI, blunt-ended with T4 DNA polymerase (Takara Bio, Kusatsu, Japan) treatment to eliminate ClaI site, and self-ligated, producing pBICP35 (-ClaI).

A DNA fragment containing ER targeting peptide coding region was amplified from pBICER-mCherry (Kaido et al., 2009) using primers 1 and 2. A DNA fragment containing mScarlet-i coding region was amplified from pmScarlet-i_C1 (Addgene, Watertown, MA, USA) using primers 3 and 4. These fragments were mixed and used as the template for recombinant PCR using primers 1 and 4. The amplified PCR product was digested with BamHI/KpnI and inserted into the corresponding site of pBICP35 (-ClaI), producing pBICER-mSi.

A DNA fragment containing mSi coding region was amplified from pBICER-mSi using primers 5 and 6. A DNA fragment containing p27 coding region was amplified from pUCR1 using primers 7 and 8. These fragments were mixed and used as the template for recombinant PCR using primers 5 and 8. The amplified PCR product was digested with BamHI/KpnI and inserted into the corresponding site of pBICP35 (-ClaI), producing pBICp27-mSi (Fig. S1).

A DNA fragment containing mSi peptide coding region was amplified from pBICER-mSi using primers 9 and 10. The amplified PCR product was digested with MluI/ClaI and inserted into the corresponding site of pUCR1-MsG (Kaido et al., 2009), producing pUCR1-MmSi (Fig. S1).

pUCR1-MmSi was digested with MluI/ClaI and inserted into the corresponding site of pR1-sGFP (Kaido et al., 2009), producing pR1-mSi. pR1-mSi was digested with SmaI/XhoI and inserted into the corresponding site of pUCR1, producing pUCR1-mSi (Fig. S1).

A DNA fragment containing T7 promoter and the cDNA of RCNMV (Aus) RNA2 was amplified from pRC2|G (Xiong and Lommel, 1991) using primers 11 and 12. The amplified PCR product was digested with EcoRI/SmaI and inserted into the corresponding site of pUC119 (Takara Bio), producing pUCR2 (Fig. S1).

A DNA fragment containing T7 promoter and the cDNA of R2fsMP was amplified from pRNA2fsMP (Tatsuta et al., 2005) using primers 12 and 13. The amplified PCR product was digested with EcoRI/SmaI and inserted into the corresponding site of pUC119, producing pUCR2fsMP (Fig. S1).

2.2. Plant growth conditions

N. benthamiana expressing B2-GFP (B2-GFP plants) were grown on commercial soil (Sumirin-Ryokka, Tokyo, Japan) at 25 ± 2 °C and under long-day conditions with 16 h illumination per day. 4- or 5-week-old plants were used for viral RNA inoculation and 5- or 6-week-old plants were used for agroinfiltration or inhibitor treatment.

2.3. Inoculation of plants with viral RNA

RCNMV RNA was transcribed *in vitro* from plasmids given the prefix 'pUC' by using T7 RNA polymerase (Takara Bio) and the concentration of RCNMV was adjusted to 1.0 μg/μl. 4- or 5-week-old wt *N. benthamiana* or B2-GFP plants were rub-inoculated with a mixture of *in vitro* transcripts of RCNMV RNA by using carborundum (Nacalai Tesque, Kyoto, Japan) and incubated at 17 °C under long-day conditions with 16 h illumination per day.

2.4. Microscopy

Subcellular localization of proteins tagged with FPs was observed using an Olympus FluoView FV1200 confocal laser scanning microscope (CLSM). A 40 × Plan Apo objective lens (numerical aperture 0.95) or 60 × Plan Apo (numerical aperture 1.35) oil immersion objective lens (Olympus, Tokyo, Japan) was used. Excitation dichroic mirrors DM405/473/559, beam splitter SDM560 for GFP and mirror for RFP, and variable barrier filters (VBF) of 485 nm–545 nm for GFP and 570 nm–670 nm for RFP were used for the detection of fluorescent signals. In experiments for visualizing dual fluorescence, images were taken in a sequential mode to minimize fluorescent signal leakage. Images were stacks composed of optical sections taken at 1–2 μm intervals or single section taken at a cortical region of a plant cell. In time lapse imaging analyses, images were taken at every 1–10 s. All images were processed using Image J/Fiji (ver. 1.52p) (https://imagej.net/software/fiji/) (Schindelin et al., 2012).

The spread of mScarlet-i fluorescence was observed using Zeiss Axio Observer 7 fluorescence microscope using the imaging program ZEN 3.1 pro (Carl Zeiss, Oberkochen, Germany).

2.5. Northern blot analysis

Total RNA extraction from wt *N. benthamiana* or B2-GFP plant leaves and northern blot analysis were performed as described previously (Mizumoto et al., 2003). Probes used for detection of positive-strand RCNMV RNA1 and RNA2 were as described by Mizumoto et al. (2002). The luminescence signal was detected by using a WES-6100 Lumino Graph (ATTO, Osaka, Japan) and the signal intensity was calculated by using Image J/Fiji (ver. 1.52p).

2.6. Inhibitor treatment of plants

Half leaf of 5- or 6-week-old plants was infiltrated with 5 μM Latrunculin B (Lat B; Sigma-Aldrich, St. Louis, U. S. A.) in 0.2% dimethyl sulfoxide (DMSO; FUJIFILM Wako Pure Chemical, Osaka, Japan) 6 h in advance of RCNMV inoculation. Plants were inoculated with *in vitro* transcripts of RCNMV and incubated at 17 °C. The other half leaf was infiltrated with 0.2% DMSO as a control treatment.

2.7. Staining of nucleus

5-week-old B2-GFP plants were infiltrated with 4′–6′-Diamidino-2-phenylindole (DAPI; Tocris bioscience, Bristol, U.K.) in phosphate-buffered saline buffer (PBS; Takara Bio) 20 min before observation and incubated at room temperature.

2.8. Agroinfiltration of plants

5- or 6-week-old B2-GFP plants were infiltrated with *Agrobacterium tumefaciens* GV3101 strain (pMP90) containing plasmids given the prefix 'pBIC'. In the localization analysis experiment of p27-mSi, plants were incubated in a moist chamber at 22 °C for 2 days. In the localization analysis experiment of ER-mSi, plants were incubated in a moist chamber at 22 °C for 1 day and rub-inoculated with a mixture of *in vitro* RCNMV transcripts. After inoculation, plants were incubated in a moist chamber at 17 °C for 20–28 h.

2.9. Image analysis

2.9.1. Number and size

After the images were taken and acquired in TIFF format using CLSM, only the infected cells were trimmed using GNU Image Manipulation Program (GIMP; ver. 2.10.20) (https://www.gimpo.org/) and used for image analysis. Three images were used to create a classifier using Trainable Weka Segmentation (TWS) plug-in (https://imagej.net/plugins/tws/) (Arganda-Carreras et al., 2017) for Image J/Fiji. To confirm its effectiveness, the three test images were segmented by each classifier. The same classifier was applied to all images taken at the same experiment. After identifying dsRNA structures, inverting images into 8-bit type and binarizing them to generate binary images, fill hole and analyze particle plug-in for Image J/Fiji were performed to measure the number and size of dsRNA structures.

2.9.2. Velocity

Sequential images were taken at three infected sites and subjected to image analysis. After randomly selecting 10 structures per site, we calculated the mean velocity of each structure using MTrack J plug-in (https://imagej.net/plugins/mtrackj) (Meijering et al., 2012) for Image J/Fiji.

2.9.3. RGB intensity

Relative intensities of red and green fluorescent signal were calculated using the RGB profiler plug-in (https://imagej.nih.gov/ij/plugins/rgb-profiler.html).

3. Results

We define subcellular structures containing fluorescent proteins as follows. Granules and punctates are fluorescent structures smaller than 1.0 μm^2. Spot-like structures are between 1.0 μm^2 and 20 μm^2 in size. The aggregates represent fluorescent structures larger than 20 μm^2 in size.

3.1. B2-GFP based-live imaging revealed the subcellular dynamics of RCNMV dsRNA granules

A previous report showed that B2-GFP localized to larger cytoplasmic aggregates or smaller granules formed only during viral infection (Monsion et al., 2018). First, we ascertained whether similar structures could be observed during RCNMV infection using CLSM. In mock-inoculated leaves, B2-GFP localized to the nucleus and spread uniformly throughout the cytoplasm in the epidermal cells (Fig. S2, left

panel and Fig. S3A). On the other hand, cytoplasmic small granular structures and large aggregates were observed in the leaves inoculated with wild type RCNMV RNA transcripts (RNA1 + RNA2) at 24 h post inoculation (hpi) (Fig. S2, right panel). Interestingly, nuclear GFP signal in the cells with those aggregates tended to be much weaker than that in mock-inoculated leaves (Fig. S2 and S3). In the virus-infected cells, B2-GFP might re-localize from nucleus to the cytoplasmic aggregates. Cytoplasmic aggregates and nucleus are easily distinguishable on the basis of their shapes and brightness (Fig. S3B). These structures, which are formed specifically during viral infection, are thought to be the sites where dsRNA, a component of VRCs, is synthesized. Since B2-GFP binds to the dsRNA, which is a viral replication intermediate, it is possible that B2-GFP affects viral multiplication. To assess this possibility, we compared the accumulation of RCNMV RNA in wt *N. benthamiana* plants with that in B2-GFP plants at 2 days post inoculation (dpi; inoculated leaves) and 7 dpi (systemic leaves). Similar amounts of positive-stranded viral RNA accumulated in both plants (Figs. S4A–S4C). These results suggest that B2-GFP neither inhibited nor promoted viral replication and that B2-GFP plants are favorable for monitoring the dynamics of RCNMV dsRNA structures.

The dynamics of viral dsRNA were monitored in the RCNMV-inoculated leaves of B2-GFP plants over time using CLSM. Numerous dsRNA granules started to appear in the cortical region on the upper wall of epidermal cells at 5 hpi. Later, at 9 hpi and 15 hpi, larger spot-like structures of dsRNA were observed (Fig. 1, left panels). These observations suggest that dsRNA structures grow in size during viral infection. Some of the dsRNA structures were located along the outer edge of the epidermal cells (Fig. 1).

3.2. *The dynamics of RCNMV dsRNA granules are uncoupled from the functions of MPs*

Previous reports have shown that several viral MPs, including RCNMV MPs, colocalize with viral replicase or replication complexes (Heinlein, 2015; Tilsner and Oparka, 2012). To test whether RCNMV MPs are involved in the formation of dsRNA structures and the increase in their size, we inoculated B2-GFP plants with *in vitro*-synthesized transcripts of mutant RCNMV, which does not express MP (RNA1 +

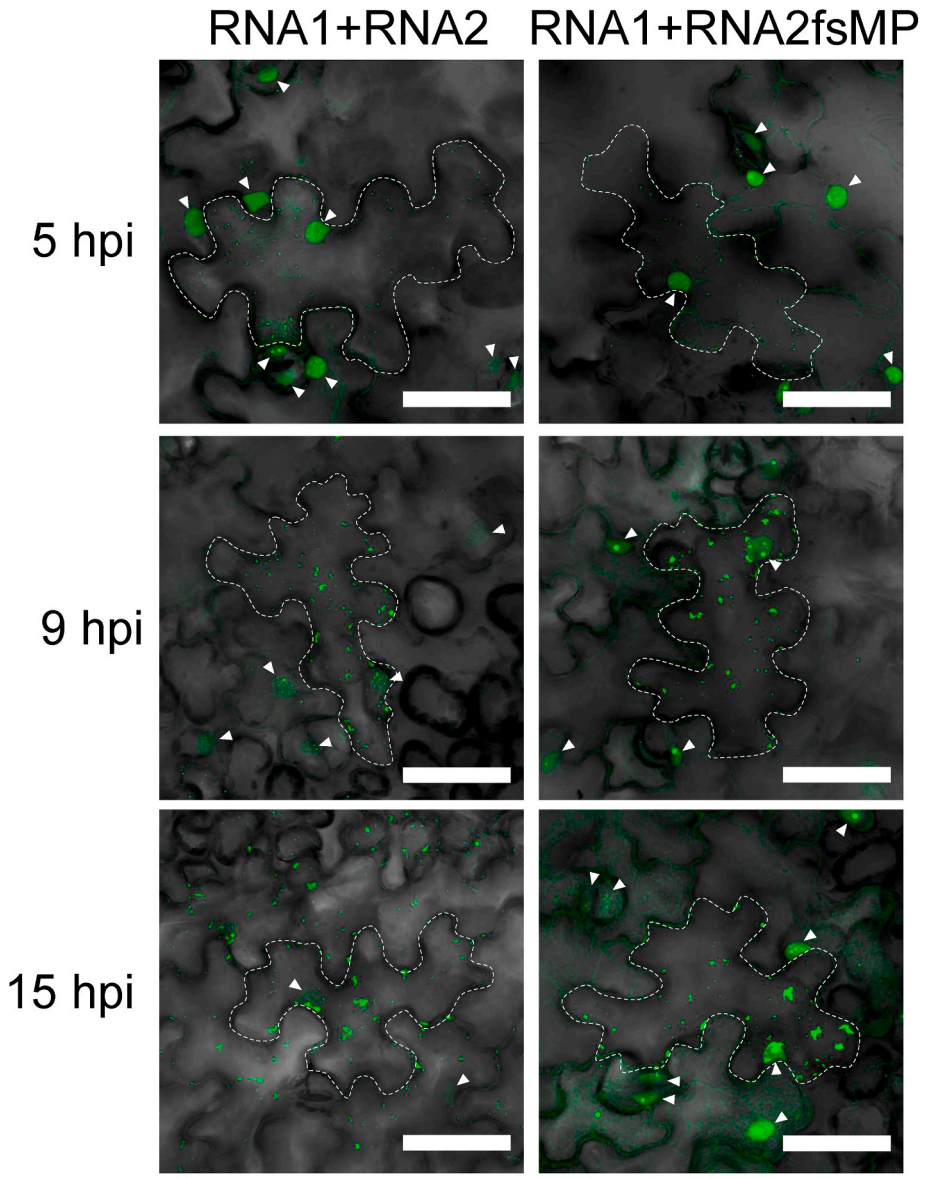

Fig. 1. Time course imaging of dsRNA structures. 5-week-old B2-GFP plants were inoculated with a mixture of RCNMV RNA1 and RNA2 (left panels) or RNA1 and RNA2fsMP (right panels), and incubated at 17 °C. Observation at 5 hpi (upper panels), 9 hpi (middle panels) and 15 hpi (lower pannels). DIC and GFP channel images were merged. Arrowheads, nucleus. Scale bars = 50 μm.

RNA2 fsMP). At 5 hpi, small dsRNA granules appeared on the inner surface of epidermal cells, and later, larger structures were detected (Fig. 1, right panels). There was little difference in the localization of the dsRNA compared with that in wt RCNMV-inoculated leaves.

The number and size of dsRNA structures were assessed by using the trainable weka segmentation (TWS) program. The number of dsRNA structures gradually increased over time (Fig. 2A). Larger dsRNA structures appeared over time. The Steel–Dwass multiple-comparison test detected significant differences in the size of dsRNA structures between at 5 and 9 hpi for wt or fsMP mutant RCNMV (Fig. 2B, left panel). The median value remained almost the same, but the mean value gradually increased. This suggests that over the course of infection, small new dsRNA granules are continuously formed and existing dsRNA granules are gradually enlarged (Fig. 2B, right panel). Since a few conspicuous larger structures than 5 μm^2 in size were found to be formed in infected cells, we focused on the largest structures in each cell and compared them between each time point. The mean size of the largest structures in infected cells increased significantly every 4–5 h (Fig. 2C). We confirmed that there was no significant difference between the size of dsRNA structures in the wt RCNMV- and fsMP mutant-infected cells. These results indicate that the formation of VRCs and the increase in their size are independent of RCNMV MPs.

3.3. An actin antagonist inhibited the intracellular transport and aggregation of dsRNA granules

To examine how dsRNA granules grow in size, we performed the time-lapse tracking of dsRNA granules under high magnification. B2-GFP plants were inoculated with wt RCNMV and subjected to time-lapse imaging analysis at 5 hpi. We observed the active movement of dsRNA granules smaller than 1.0 μm^2 in size (Video S1) and sometimes larger dsRNA spot-like structures as well. Notably, small punctate granules were observed to move and coalesce with the larger ones (Fig. 3). This suggests that some dsRNA granules are highly mobile and that the larger aggregates may be formed as small granules coalesce each other and grow in size over time. These small granules looked to move with the ER streaming (Fig. S5, Video S2).

Supplementary video related to this article can be found at https://doi.org/10.1016/j.virol.2022.01.015

Latrunculin B (Lat B), an inhibitor of actin polymerization, prevented the intracellular transport of TMV VRCs (Liu et al., 2005). To ascertain the involvement of the acto–myosin system in the intracellular transport of RCNMV dsRNA granules, we treated the leaves with Lat B and observed the subcellular localization of dsRNA structures. In the negative control, i.e., dimethyl sulfoxide (DMSO)-treated leaves, dsRNA

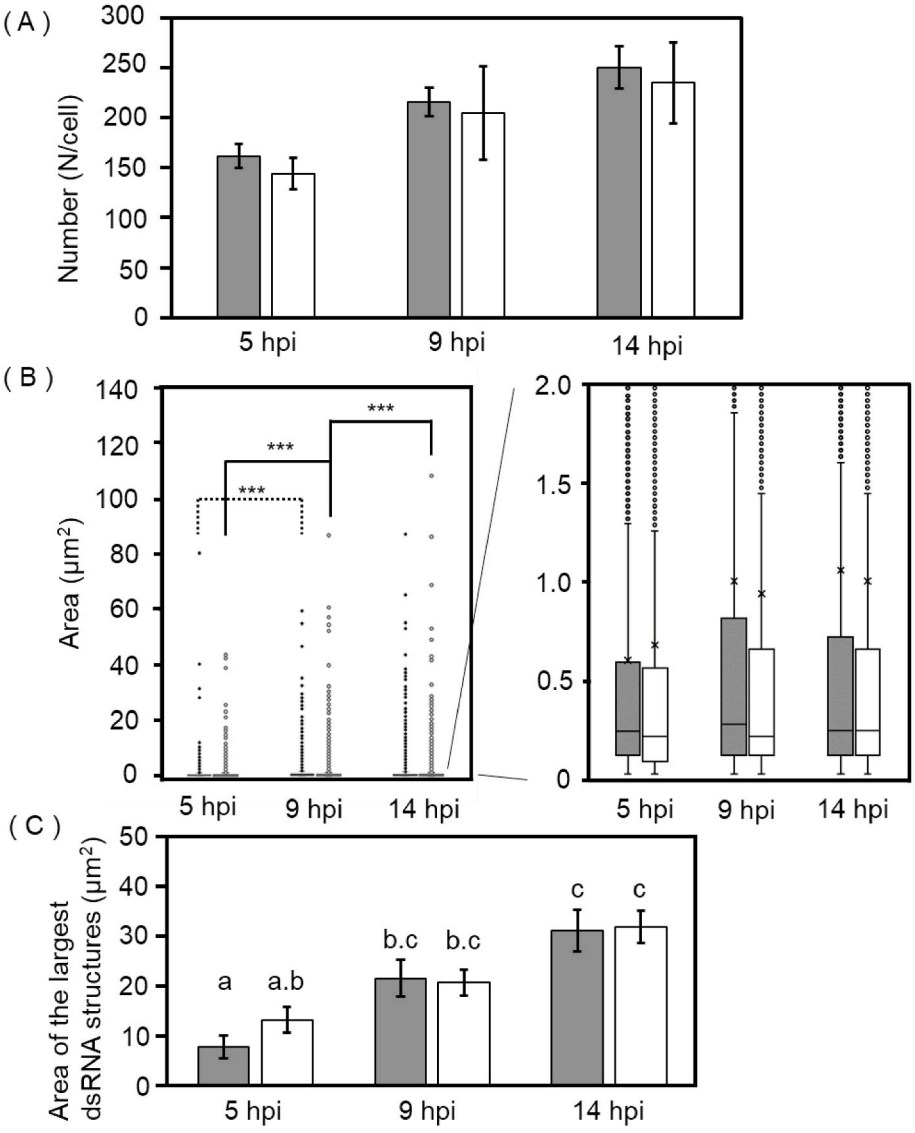

Fig. 2. Number and area of dsRNA structures. 4-week-old B2-GFP plants were inoculated with a mixture of RCNMV RNA1 and RNA2 (gray) or RNA1 and RNA2fsMP (white), and incubated at 17 °C. Confocal microscopy images were taken at 5 hpi, 9 hpi and 14 hpi. Ten images were subjected to image analysis at each time point. The number and size of dsRNA structures were calculated by Trainable Weka Segmentation (TWS), image J plug-in tool. Results were obtained from three independent experiments. (A) The mean number of dsRNA structures per cell. (B) The area of all dsRNA structures (left graph) and dsRNA structures less than 2 μm^2 (right graph) (Steel-Dwass test: ***, $P < 0.001$). × in the right box plot shows the mean of the size. (C) The mean area of the largest structures in infected cells. Significantly different statistical groups indicated by two-way ANOVA with post-hoc Tukey's honest significance test were shown with different capital letters ($P < 0.05$).

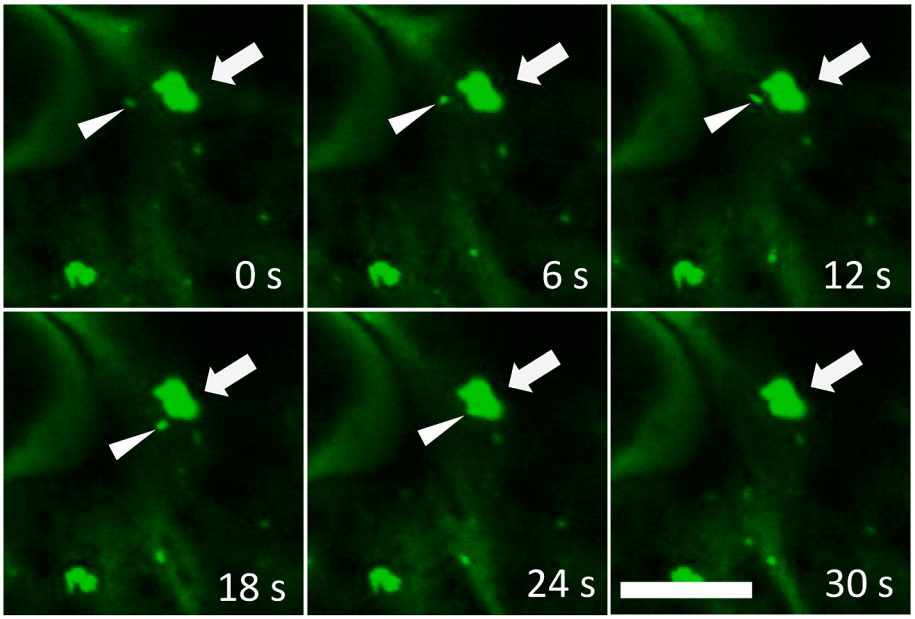

Fig. 3. Time lapse imaging showing dsRNA structures and fusion event. 4-week-old B2-GFP plants were inoculated with a mixture of RCNMV RNA1 and RNA2 and incubated at 17 °C. Sequential images of the same focus were taken every 6 s at 5 hpi. A small dsRNA granule (arrowheads) moved and fused with bigger one (arrows).
Scale bar = 10 μm.

structures of various sizes, such as small punctates and larger aggregates, were observed at 12 hpi (Fig. 4A, left panel). Meanwhile, in Lat B-treated leaves, the size of the aggregates appeared to be much smaller than those in DMSO-treated leaves (Fig. 4A, right panel). Image analysis detected no significant difference between the number of dsRNA granules in the DMSO-treated and Lat B-treated leaves (Fig. 4B). However, a significant difference in the size of dsRNA granules was detected between the two treatments. Few aggregates larger than 10 μm^2 in size were detected after the Lat B treatment (Fig. 4C). In addition, the mean size of the largest dsRNA structures was reduced to 30% in the Lat B-treated leaves compared with that in the DMSO-treated leaves (Fig. 4D).

Next, to investigate whether Lat B affects the intracellular transport of dsRNA granules, we performed time-lapse imaging analysis. The dsRNA granules moved actively in DMSO-treated leaves (Fig. 5A (left panel), Video S3); little intracellular movement was observed in the Lat B-treated leaves (Fig. 5A (right panel), Video S4). The velocity of dsRNA granules was calculated using Mtrack J. The average velocity after Lat B treatment was reduced to 17.0% of that after DMSO treatment (Fig. 5B). These results suggest that the acto–myosin system is involved in the intracellular transport of dsRNA granules and their subsequent aggregation. Lat B treatment in this experimental condition did not affect the accumulation level of RCNMV RNAs in the inoculated leaves (Fig. S6). The result suggests that the formation of large dsRNA aggregates is not a prerequisite for the higher accumulation of viral RNA accumulation of RCNMV. Spot-like structures shown in the right panel of Fig. 4A are probably large enough to recruit the MPs and can support cell-to-cell movement of the virus. Higher concentration of Lat B to inhibit the formation of spot-like structures or even granular structures of dsRNA might inhibit the multiplication of RCNMV.

Supplementary video related to this article can be found at doi: mmcdoino

3.4. dsRNA structures localize at the sites of viral replication

Thus far, we successfully monitored the subcellular dynamics of RCNMV dsRNA granules; however, whether viral replication occurs within dsRNA granules, especially small cortical punctates (~1 μm^2 in size), formed during RCNMV infection remains unclear, i.e., whether RCNMV dsRNA granules are components of VRCs remains unclear. Thus, we tested whether dsRNA granules colocalize with p27, the localization of which has widely been used as a marker of the RCNMV replication site (Kusumanegara et al., 2012; Hyodo et al., 2013, 2015, 2017, 2019). First, B2-GFP plants were infiltrated with a mixture of two *Agrobacterium* strains that express a fusion of p27 with an RFP, mScarlet-i (p27-mSi), and another viral replication protein, p88. No cortical dsRNA granules were observed and p27-mSi was observed as a large inclusion (Fig. 6, panels A–C). This observation is similar to the localization of p27-GFP when it is expressed alone (Kusumanegara et al., 2012). Next, B2-GFP plants were infiltrated with a mixture of three *Agrobacterium* strains that expressed p27-mSi and p88 and RNA2 as the template for viral RNA replication. Infiltration of this combination of *Agrobacterium* resulted in the accumulation of lower but substantial amount of RNA2 compared with those expressed wild type p27 and p88 and RNA2 (Fig. S7A), showing that p27-mSi is functional. The fluorescence of p27-mSi was observed as small punctates or slightly large spot-like structures (Fig. 6, panel E), or large nuclear-sized aggregates (Fig. 6, panel H). Importantly, these red signals coincided with the green dsRNA signals (Fig. 6, panels D–I). At a high magnification, larger aggregates, as well as most tiny granules smaller than 1 μm^2 in size also showed signals of both p27-mSi and B2-GFP (Fig. 6, panels J–L). We calculated the relative intensities of GFP and RFP signals by using an RGB profiler. The green signals of B2-GFP and red signals of p27-mSi were found to overlap in both the tiny dsRNA granules and aggregates (Fig. S8). These results indicate that the cortical punctates detected by B2-GFP are components of the VRC and localize at the sites where viral replication occurs.

RCNMV replication is associated with the ER membrane (Hyodo and Okuno, 2016, 2020). It is reasonable to assume that dsRNA granules colocalize with the cortical ER. Thus, we expressed the mSi tagged with an ER-targeting peptide (ER-mSi) via *Agrobacterium* infiltration and inoculated the leaves of B2-GFP plants with *in vitro* transcripts of wt RCNMV. In mock-inoculated leaves, the ER-mSi localized at reticulated structures around the cortical region on the upper wall of epidermal cells (Fig. 7A, panels a–c), while in RCNMV-inoculated leaves, ER-mSi also localized at the aggregates and overlapped with B2-GFP (Fig. 7A, panels d–f). At high magnification, a large aggregate (approximately 20 μm^2 in size) that merged well with the proliferated ER was observed (Fig. 7A, panels g–i). On the other hand, interestingly, tiny punctates (approximately 0.5 μm^2 in size) did not colocalize with, but rather, localized adjacent to, intact ER tubules (Fig. 7A, panels j–l). We then calculated the relative intensities of GFP and RFP using an RGB profiler. The GFP

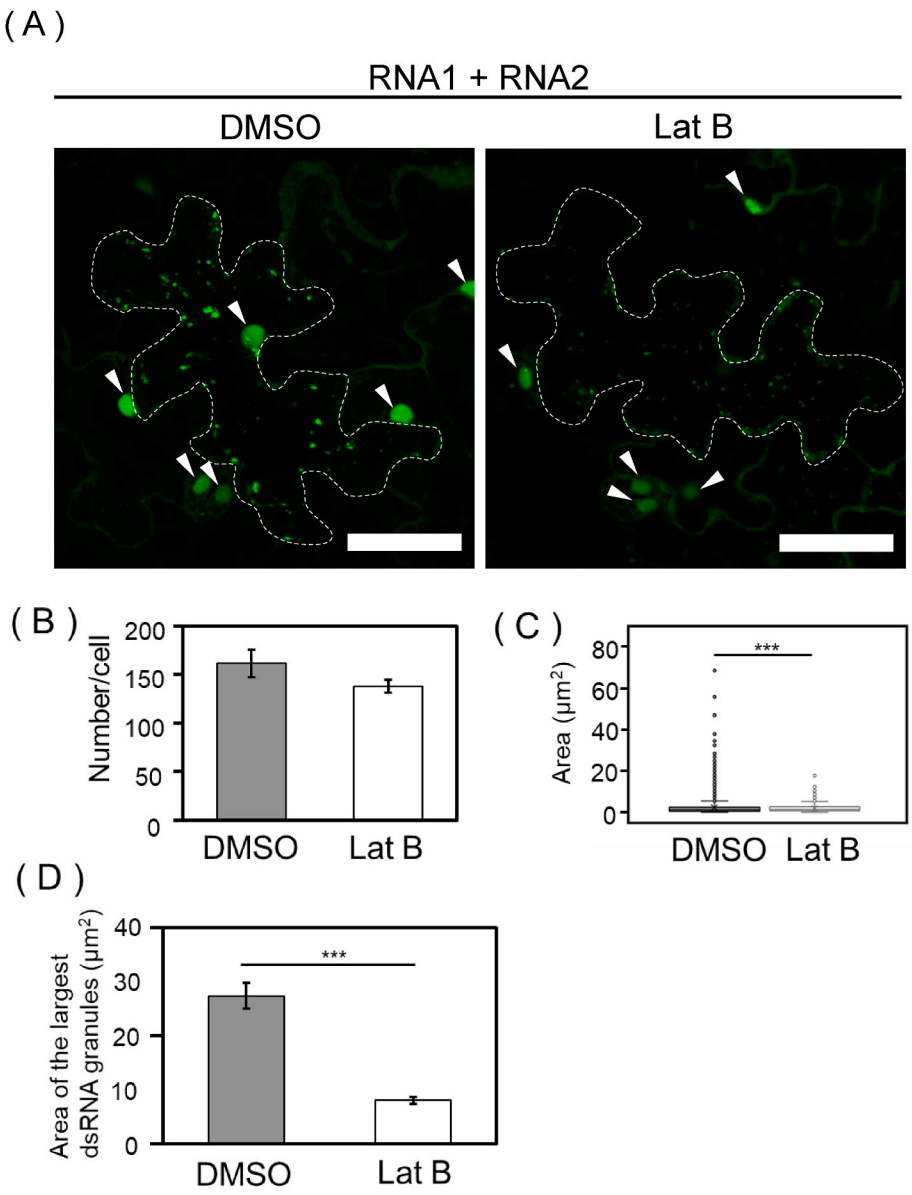

Fig. 4. Effect of Latrunculin B on subcellular localization of dsRNA structures. 5-week-old B2-GFP plants were infiltrated with DMSO solution (0.2% DMSO/DW) or Latrunculin B (Lat B) solution (5 μM Lat B in 0.2% DMSO/DW), followed by mechanical inoculation 6 h later with a mixture of RCNMV RNA1 and RNA2. Ten images were subjected to image analysis using TWS. Results were obtained from three independent experiments. (A) Representative confocal microscopy images of inoculated leaves at 12 h post inoculation. Scale bars = 50 μm. Arrowheads, nucleus. (B) The mean number of dsRNA structures per cell. (C) The area of all dsRNA structures (Wilcoxon rank sum test: ***, $P < 0.001$). (D) The mean size of the largest dsRNA structures (Welch's *t*-test: ***, $P < 0.001$).

signals of the dsRNA aggregates almost overlapped with the RFP signals, while the GFP signals of the tiny dsRNA granules hardly overlapped with the RFP signals (Fig. 7B). These results suggest that punctate dsRNA granules formed at an early infection stage localize adjacent to the ER membrane, and later, they grow larger, involving the ER membrane, to form relatively larger aggregates.

3.5. MPs preferentially colocalized with larger VRCs

Using an immunofluorescent labeling method, we previously reported that RCNMV MPs colocalized with cortical VRCs containing viral dsRNA; this colocalization is essential for efficient viral cell-to-cell movement (Kaido et al., 2014). To assess the colocalization of the MPs with dsRNA in living cells within B2-GFP plants, we used *in vitro* transcripts of the recombinant RCNMV (RNA1-MmSi + RNA2fsMP), which expressed the fusion protein of MP and mScarlet-i (MP-mSi). We also used *in vitro* transcripts of the recombinant RCNMV (RNA1-mSi + RNA2fsMP) that expressed free mSi as the negative control (Fig. S1B). In contrast to the negative control-inoculated leaves, the RFP signal spread to multiple cells by 42 h after inoculation in the leaves inoculated with RNA1-MmSi + RNA2fsMP, confirming that MP-mSi retains the ability to transport viral RNA to adjacent cells (Fig. S7B).

In the negative control-inoculated leaves, B2-GFP localized at both the small punctates and larger aggregates. Free mSi localized at the nucleus and widely distributed in the cytoplasm, but did not colocalize with dsRNA structures (Fig. 8, panels A–C). Per the observation of the leaves inoculated with RNA1-MmSi + RNA2fsMP at 600 × magnification, cortical dsRNA structures were observed as both the small punctates and large aggregates. The RFP signals of MP-mSi overlapped almost perfectly with those of the spot-like structures and the large aggregates (>5 μm^2 in size) of B2-GFP (Fig. 8, panels D–F). Interestingly, however, when the image was enlarged for observation, many tiny dsRNA granules that did not colocalize with MP-mSi were detected (Fig. 8, panels G–I). Observation at 3000 × magnification more clearly confirmed the presence of many tiny dsRNA granules (approximately 0.5 μm^2 in size) that did not colocalize with MP-mSi. We also observed tiny granular structures containing only the red signals of MP-mSi; these signals did not overlap with the green signals of the dsRNA structures (Fig. 8, panels J–L). Analysis using the RGB profiler confirmed the presence of three types of granular structures: those containing only GFP

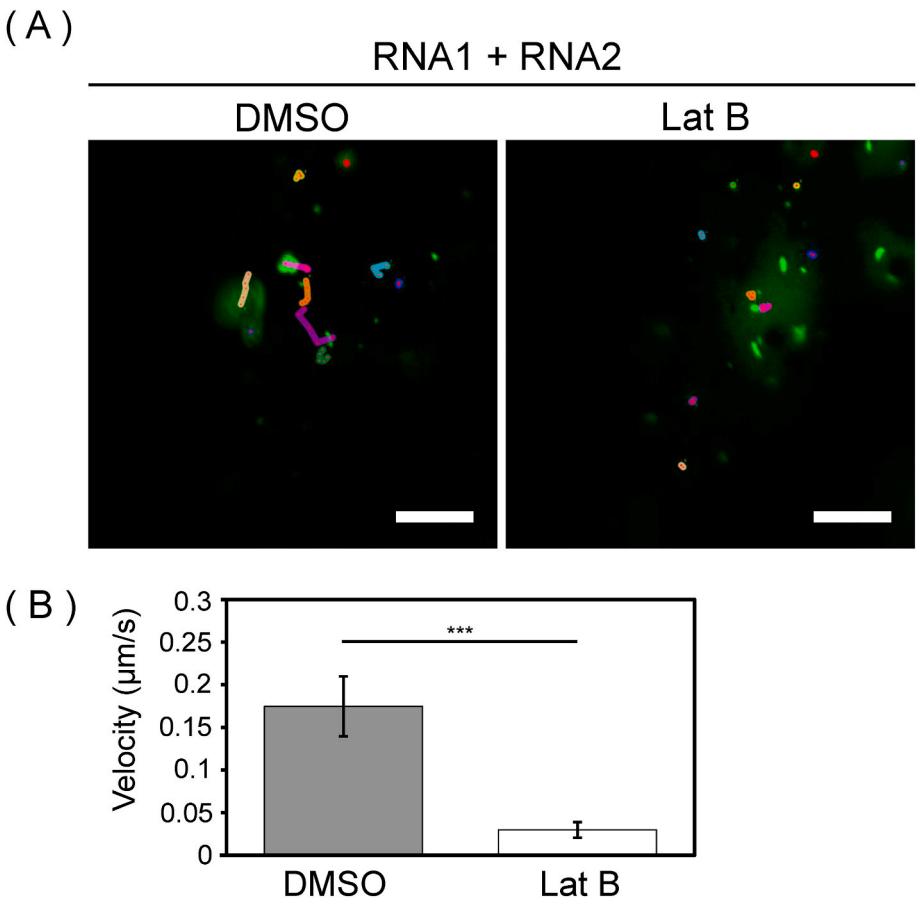

Fig. 5. Effect of Latrunculin B on intracellular movement of dsRNA structures. 5-week-old B2-GFP plants were infiltrated with DMSO solution (0.2% DMSO/DW) or Latrunculin B (Lat B) solution (5 μM Lat B in 0.2% DMSO/DW), followed by mechanical inoculation 6 h later with a mixture of RNA1 and RNA2. (A) Sequential images were taken every 1.6 s for 8.0 s at 13 h post inoculation. Tracks, represented by different colors, of randomly selected 10 dsRNA structures were imaged by using Mtrack J, image J plug-in tool. Scale bars = 10 μm. (B) Sequential images were taken every 3.2 s for 16.0 s at 13 h post inoculation. 3 images of infected cells were taken at each treatment and subjected to image analysis. The average velocity of randomly selected 10 dsRNA structures per each image was calculated by using Mtrack J. Each bar represents the mean velocity of dsRNA structures from three independent experiments (Welch's *t*-test: ***, $P < 0.001$). (For interpretation of the references to color in this figure legend, the reader is referred to the Web version of this article.)

signals (Fig. S9B), those containing both GFP and RFP signals (Fig. S9C), and those containing only RFP signals (Fig. S9D). We counted granules smaller than 0.5 μm^2 in size and found that yellow granules that are supposed to contain both dsRNA and MP-mSi accounted for less than 50% of the total granules (data not shown).

These observations suggest that MP-mSi can form tiny granule structures by itself and that MP-mSi has a weak association with tiny dsRNA granules, while MP-mSi colocalizes more frequently with larger spot-like structures and dsRNA aggregates.

4. Discussion

In this study, we tried to reveal the subcellular dynamics of VRCs. We judged that RCNMV VRCs can be monitored via dsRNA granules based on the following two points: First, RCNMV infected both B2-GFP and wt *N. benthamiana* plants similarly. Second, the replication protein p27 colocalized with the dsRNA granules (Fig. 6); this showed that dsRNA granules are components of VRCs. dsRNA granules were formed in the close vicinity of cortical ER tubules at an early stage of infection and were transported through the cytoplasm; this led to the coalescence of small dsRNA granules, and thus, the dsRNA granules grew in size over time to form aggregates (Figs. 1–3, 7). The formation of such aggregates may have depended on the acto–myosin system (Figs. 4 and 5). Thus, we presented an example of the detailed process of VRC formation and maturation.

We detected the fusion of dsRNA structures (Fig. 3, Video S1). It should be noted that these results do not exclude other possibilities. For example, it is possible that tiny granular VRCs recruit VRC component proteins to grow larger. However, considering that only one or a few nuclear-sized aggregate VRCs were finally formed in an infected cell (Fig. 6G–L, Kaido et al., 2014, data not shown), it seems likely that the fusion of granular VRCs substantially contributes to the growth of VRCs. Thus, larger aggregated VRCs formed in the late stage of infection contained ER (Fig. 7). p27 interacts with the host phospholipase D, which has an ability to modify the lipid composition of the ER membrane and enhances the affinity of p27 for the ER membrane (Hyodo et al., 2015). This would help the VRCs to be incorporated into the ER in the later infection stage.

The results obtained in this study suggest that the acto–myosin system drives the intracellular movement of VRCs containing dsRNA, and the VRCs grow in size by fusing with one other. TMV VRCs, which contain replication enzymes and viral RNA, have been also reported to increase during viral infection. Actin and class XI myosin are involved in the intracellular transport of VRCs in TMV (Amari et al., 2014; Liu et al., 2005). In addition, the intracellular movement of granular structures derived from the nucleocapsid protein of fig mosaic virus (FMV) and the P6 of cauliflower mosaic virus (CaMV), both of which are probably components of VRCs, is also inhibited by Lat B infiltration. These results suggest that the VRCs of these viruses also move by using the acto–myosin system (Alers-Velazquez et al., 2021; Ishikawa et al., 2015; Luo et al., 2020; Schoelz and Leisner, 2017). Given that FMV and CaMV are negative-sense RNA and dsDNA viruses, respectively, while TMV and RCNMV are positive-sense RNA viruses, the mechanism underlying the intracellular trafficking of VRCs may be widely conserved among plant viruses.

TGBp1, a PVX MP, is indispensable for the formation of large aggregate structures called X-bodies, and infection with the recombinant PVX that does not express TGBp1 induced the formation of smaller-sized VRCs (Tilsner et al., 2012). On the contrary, our results showed that RCNMV MPs are neither involved in the formation of VRCs, nor in their enlargement (Figs. 1 and 2). Given that the levels of viral RNAs accumulated in the presence or absence of RCNMV MPs in *N. benthamiana*

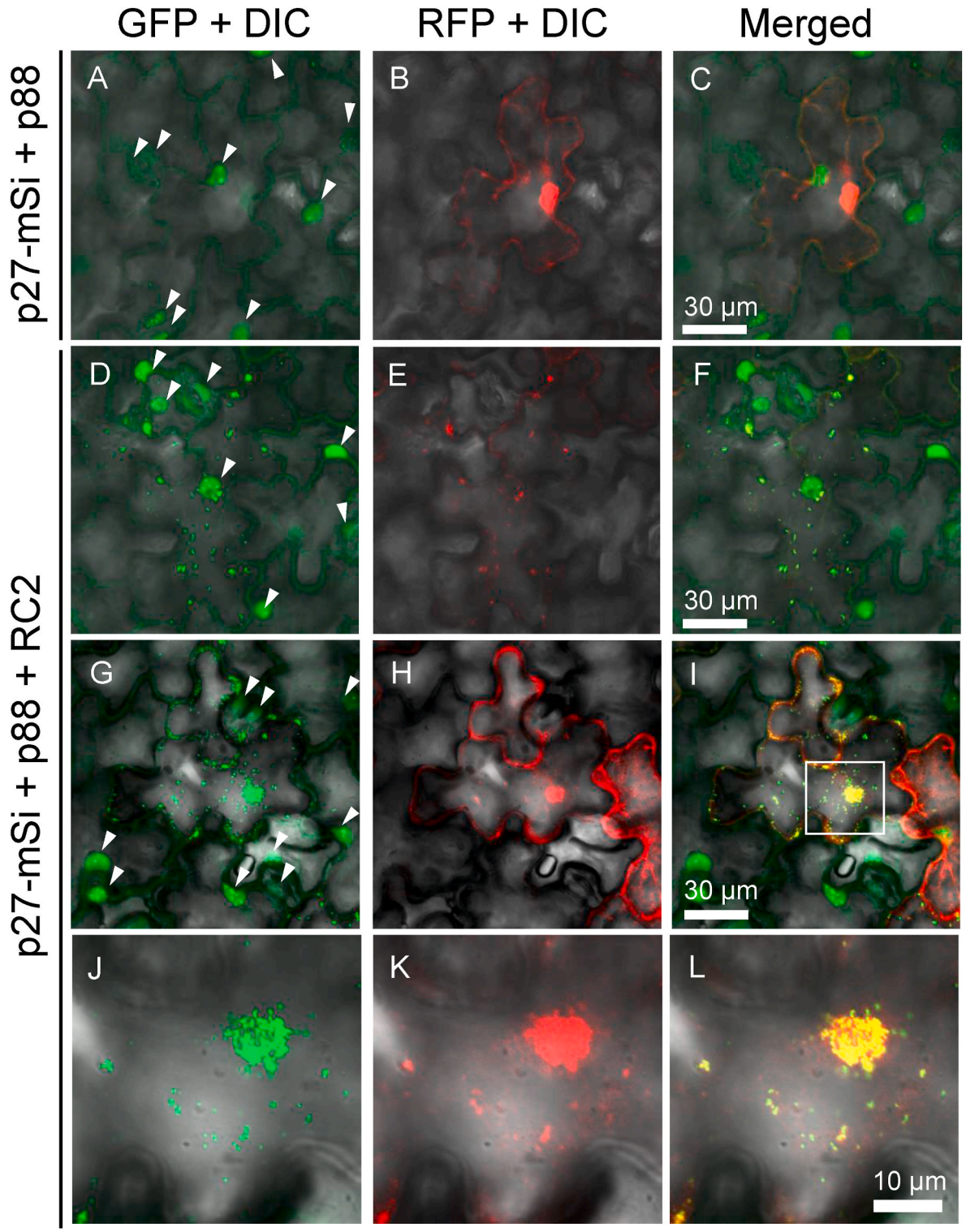

Fig. 6. Subcellular localization of p27-mSi and dsRNA structures. Representative confocal images of p27-mSi and B2-GFP localization in epidermal cells at 2 days post infiltration. *Agrobacterium* that contains pBICp27-mSi (OD_{600}=0.1) and pBICp88 (OD_{600}=0.27) together with or without pBICRC2 (OD_{600}=0.27), which expresses RNA2, were infiltrated into 5-week-old B2-GFP plants. (A–L) Images of leaves infiltrated with p27-mSi and p88 (A–C) or p27-mSi, p88 and RC2 (D–L). (D–I) Images at low magnification. (J–L) Images of the area surrounded by white line in image (I) at high magnification. In each raw, the left and middle images were taken under GFP and RFP channels for B2-GFP and p27-mSi signals, respectively. The right panels represent merged images of the left and middle images in the same raw. DIC, differential interference contrast. Arrowheads, nucleus.

protoplasts were comparable (Kaido et al., 2009), these results seem to be reasonable. In addition, RCNMV MP-GFP expressed alone from *A. tumefaciens* did not remain in the cytoplasm and was transported to the PD (Kaido et al., 2009). This result shows that RCNMV MPs have a low affinity for the ER membrane. Such intrinsic characteristics of RCNMV MP may have led to their independence from VRC formation.

In this study, we observed that MPs preferentially colocalized with relatively large structures, rather than with tiny dsRNA granules (Fig. 8).

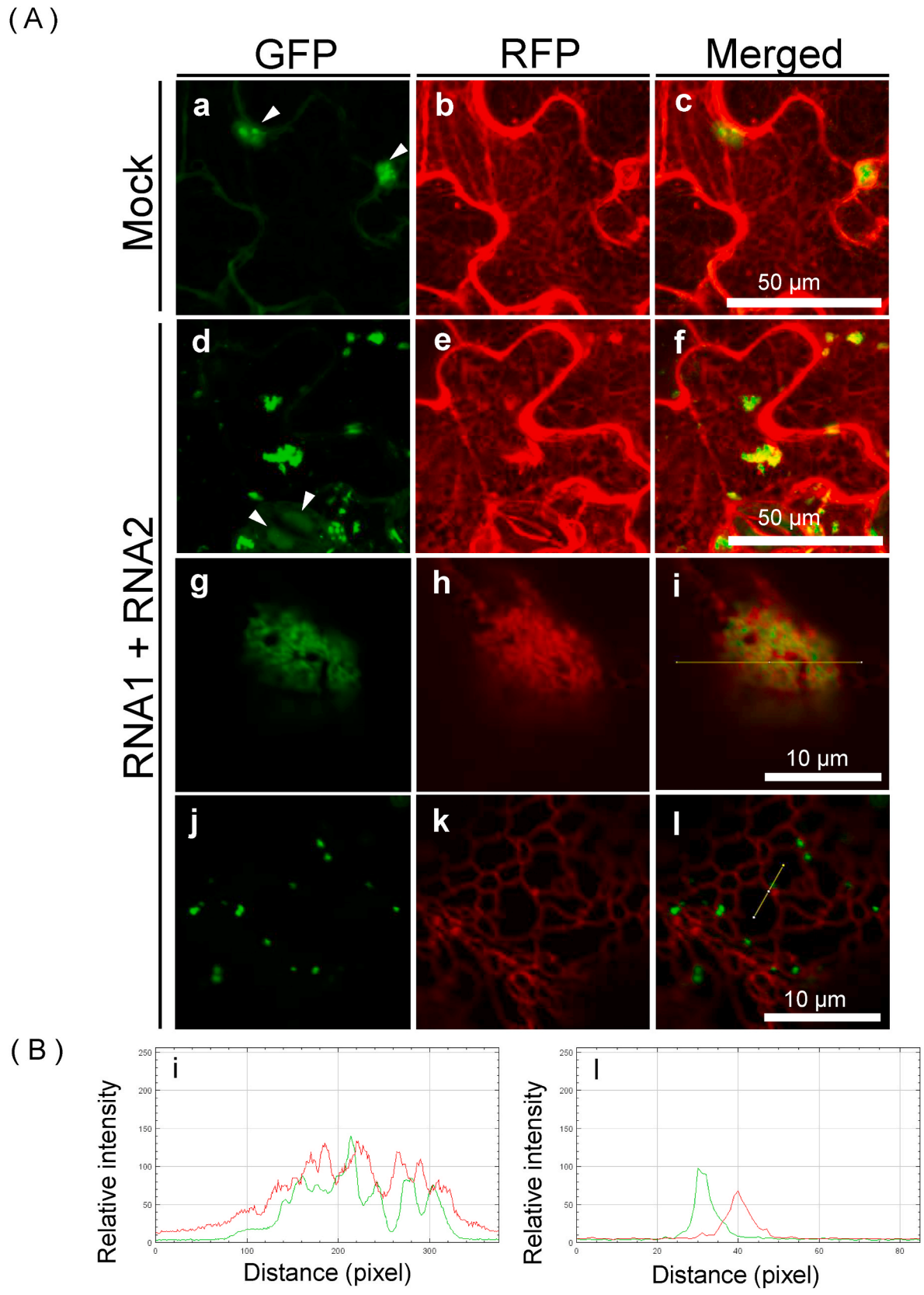

Fig. 7. Subcellular localization of ER-mSi and dsRNA structures. (A) *Agrobacterium* that contains pBICER-mSi (OD_{600}=0.4) was infiltrated into 5-week-old B2-GFP plants and incubated at 22 °C. 1 day later, plants ware mechanically inoculated with mock (a–c) or a mixture of RCNMV RNA1 and RNA2 (d–l), and incubated at 17 °C for approximately 1 day. Observation of dsRNA structures at low magnification (d–f). Observation of a larger aggregation (g–i) and tiny dsRNA granules (j–l) under high magnification. Arrowheads, nucleus. For others, refer to the legend for Fig. 6.(B) RGB profiles of lines in image (i) and image (l).

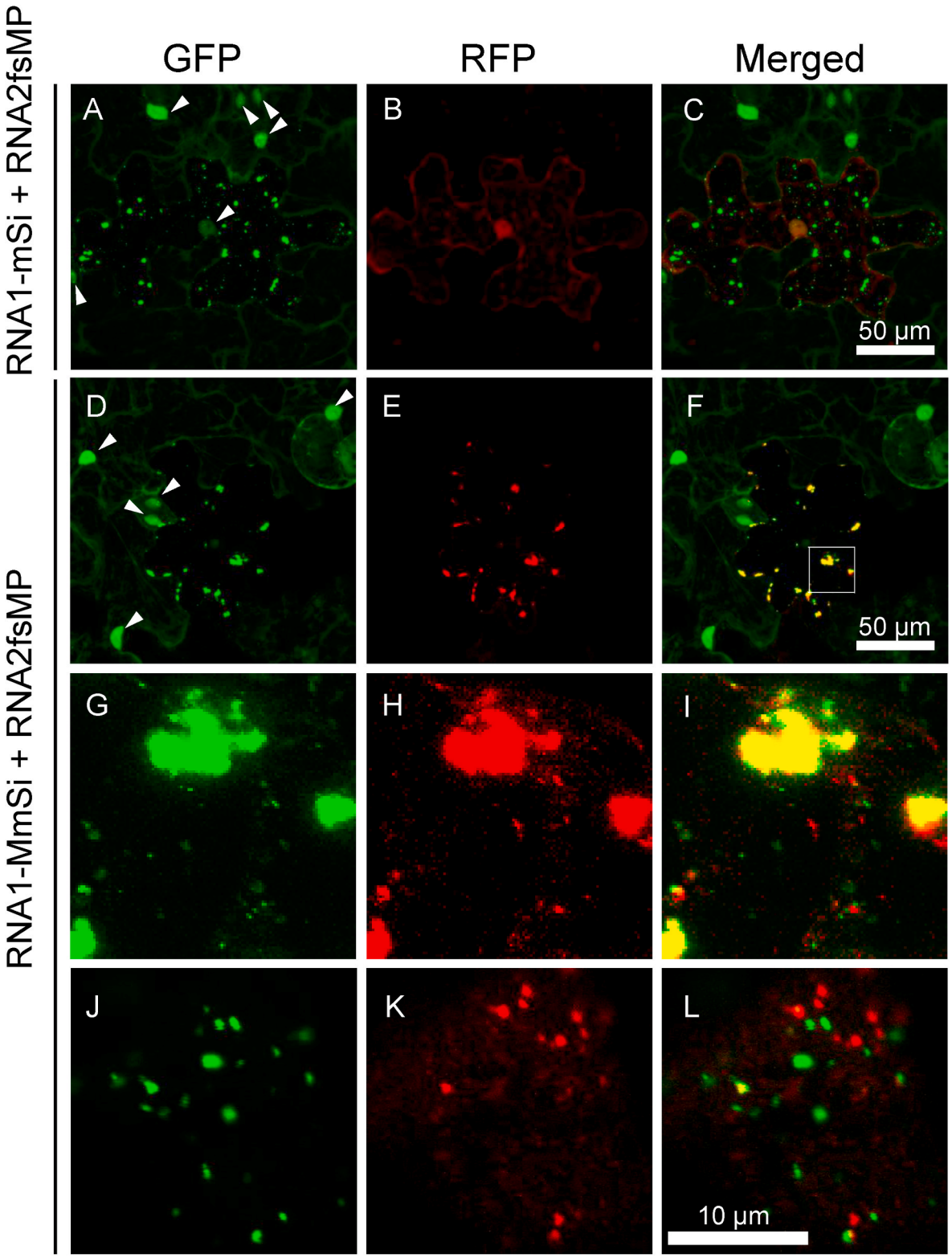

Fig. 8. Subcellular localization of mSi, MP-mSi and dsRNA structures. 4-week-old B2-GFP plants were mechanically inoculated with a mixture of RNA1-mSi and RNA2fsMP or RNA1-MmSi and RNA2fsMP, and incubated at 17 °C for 16 h. All images are confocal projections composed of about 10 optical sections taken at 1.5 μm intervals, which range from the surface to the middle of epidermal cells. Each panel represents images of leaves inoculated with RNA1-mSi and RNA2fsMP (A–C) and RNA1-MmSi and RNA2fsMP (D–L). (D–F) Observation at low (600×) magnification. (G–I) Enlarged imanes of the area surrounded by white line in image (F) (0.3% contrast-enhanced images). (J–L) Observation at high (3,000×) magnification. Arrowheads, nucleus. For others, refer to the legend for Fig. 6.

In other words, larger VRCs have greater affinity for MPs. So how do MPs colocalize with large VRCs? We observed tiny granular structures of MPs that did not colocalize with dsRNA structures (Fig. 8). This result suggests that newly translated MPs interact with each other to form MP granules and are later recruited to large VRCs. We assume two hypotheses regarding the colocalization of MPs with large VRCs: 1) MP-granular structures may move along the actin–ER network into large VRCs, which contain aggregated ER (Fig. 7). Experiments involving the inhibition of myosin function by using motor domain-deficient myosins suggest that class XI and Ⅷ myosins are involved in the subcellular movement of TMV MP punctates (Amari et al., 2014). Like TMV MPs, RCNMV MPs may be also transported through the cytoplasm via the host myosin motor protein. Aggregation of the actin–ER network may increase the frequency of encounters between VRCs and MPs. 2) MP granules may interact and colocalize with host proteins preferentially present in larger VRCs. As the VRCs mature, the accumulation of host proteins required for viral cell-to-cell movement may increase in the VRCs. This may give rise to a strong affinity between the MPs and host proteins, which may lead to the recruitment of MPs to relatively larger VRCs. MPs and VRCs may be colocalized either via the mechanisms described in points 1) or 2) or via both these mechanisms.

Results from our previous studies showed that ectopically expressed RCNMV MP-GFP colocalized with the VRCs that replicate RNA1 (Kaido et al., 2009) and that their co-localization is essential for the cell-to-cell movement of the virus (Kaido et al., 2011, 2014). Considering these results and the results of the present study, this colocalization is assumed to be important in that the MPs capture viral genomic RNAs, especially, RNA1 that does not encode MPs, for their transportation to the neighboring cells. However, how MPs transport the viral genomic RNA to the PD remains unknown. As RCNMV moves to the neighboring cell without the CP, MP-RNA complexes or components of the VRC are supposed to be transported to the PD. The VRCs of several viruses, including tobamoviruses, PVX, and TuMV, are formed at the entrance of the PD (Chai et al., 2020; Levy et al., 2015; Szecsi et al., 1999; Tilsner et al., 2013). These may function towards the co-replicational movement of the viral genome (Levy and Tilsner, 2020; Wu and Chen, 2020). We also detected some RCNMV VRCs that were formed along the outer edge of epidermal cells (they might be in close proximity to PD), while most VRCs were distributed around the cortical region on the upper wall of epidermal cells (Fig. 1). Our data do not support or deny the co-replicational movement of viruses. To prove the substantial contribution of VRCs at the entrance of the PD towards the cell-to-cell movement of the virus, we need to identify the conditions in which both the formation of VRCs at the entrance of the PD and the viral cell-to-cell movement are inhibited.

Finally, the varying subcellular localizations of viral proteins and dsRNA raise new questions about how dsRNA and MP granules are formed. Liquid–liquid phase separation (LLPS) is a phenomenon in which a homogeneous mixture of molecules changes from a one-phase liquid state to a two-phase distinguishable liquid state (Alberti and Dormann, 2019; Hyman et al., 2014). In addition to some studies showing that LLPS is involved in the multiplication of animal viruses (Guseva et al., 2020; Heinrich et al., 2018; Nikolic et al., 2017), a recent study revealed that the p26 MP of the pea enation mosaic virus 2 (PEMV2) shows phase separation into droplets *in vivo*, and may lead to viral movement (Brown et al., 2021). These findings suggest that LLPS may be a crucial phenomenon associated with the infection of plant viruses. Amino acid sequence analysis using PrDOS (Protein DisOrder prediction system), a natively disordered site-prediction web server, suggests that RCNMV MP, p27, and p88 have putative disordered domains (Takata and Kaido, unpublished data). Therefore, it is possible that the formation of RCNMV MP granules and dsRNA granules is driven by LLPS. Further efforts are needed to clarify these possibilities and the importance of LLPS in the RCNMV infection process.

Funding

This study was supported in part by a Grant-in-Aid (16H04882) for Scientific Research B and a Grant-in-Aid (21H02199) for Scientific Research B from the Japan Society for the Promotion of Science (http://www.jsps.go.jp/). The funders had no role in study design, data collection and analysis, decision to publish, or preparation of the manuscript.

CRediT authorship contribution statement

Shota Takata: wrote the first draft of the manuscript, organised data collection, designed the study, formal analysis, and interpreted the results, edited and critically reviewed the manuscript.

Kazuyuki Mise: edited and critically reviewed the manuscript, planned and co-supervision.

Yoshitaka Takano: edited and critically reviewed the manuscript, planned and co-supervision.

Masanori Kaido: wrote the first draft of the manuscript, organised data collection, designed the study, formal analysis, and interpreted the results, edited and critically reviewed the manuscript, planned and supervision of the entire work.

Declaration of competing interest

The authors declare that they have no known competing financial interests or personal relationships that could have appeared to influence the work reported in this paper.

Acknowledgements

We thank Dr. Steven A. Lommel for providing cDNA clones of RCNMV Australian strain, including pRC2|G plasmid. We thank Dr. Christophe Ritzenthaler for providing *N. benthamiana* B2-GFP seeds. We also thank Dr. Rei Yoshimoto for critical suggestions and Dr. Shigeyuki Tanaka for technical supports.

Appendix A. Supplementary data

Supplementary data to this article can be found online at https://doi.org/10.1016/j.virol.2022.01.015.

References

Alers-Velazquez, R., Jacques, S., Muller, C., Boldt, J., Schoelz, J., Leisner, S., 2021. Cauliflower mosaic virus P6 inclusion body formation: a dynamic and intricate process. Virology 553, 9–22.

Alberti, S., Dormann, D., 2019. Liquid-liquid phase separation in disease. Annu. Rev. Genet. 53, 171–194.

Amari, K., Di Donato, M., Dolja, V.V., Heinlein, M., 2014. Myosins VIII and XI play distinct roles in reproduction and transport of tobacco mosaic virus. PLoS Pathog. 10 (10), e1004448.

Arganda-Carreras, I., Kaynig, V., Rueden, C., Eliceiri, K.W., Schindelin, J., Cardona, A., Seung, H.S., 2017. Trainable Weka Segmentation: a machine learning tool for microscopy pixel classification. Bioinformatics 33 (15), 2424–2426.

Bamunusinghe, D., Hemenway, C.L., Nelson, R.S., Sanderfoot, A.A., Ye, C.M., Silva, M.A. T., Payton, M., Verchot-Lubicz, J., 2009. Analysis of potato virus X replicase and TGBp3 subcellular locations. Virology 393 (2), 272–285.

Benitez-Alfonso, Y., Faulkner, C., Ritzenthaler, C., Maule, A.J., 2010. Plasmodesmata: gateways to local and systemic virus infection. Mol. Plant Microbe Interact. 23 (11), 1403–1412.

Brown, S.L., Garrison, D.J., May, J.P., 2021. Phase separation of a plant virus movement protein and cellular factors support virus-host interactions. PLoS Pathog. 17 (9), e1009622.

Carette, J.E., Cuhl, K., Wellink, J., van Kammen, A., 2002. Coalescence of the sites of cowpea mosaic virus RNA replication into a cytopathic structure. J. Virol. 76 (12), 6235–6243.

Chai, M., Wu, X., Liu, J., Fang, Y., Luan, Y., Cui, X., Zhou, X., Wang, A., Cheng, X., 2020. P3N-PIPO Interacts with P3 via the shared N-terminal domain to recruit viral replication vesicles for cell-to-cell movement. J. Virol. 94 (8) e01898-19.
Christensen, N., Tilsner, J., Bell, K., Hammann, P., Parton, R., Lacomme, C., Oparka, K., 2009. The 5' Cap of tobacco mosaic virus (TMV) is required for virion attachment to the actin/endoplasmic reticulum network during early infection. Traffic 10 (5), 536–551.
Cui, X., Yaghmaiean, H., Wu, G., Wu, X., Chen, X., Thorn, G., Wang, A., 2017. The C-terminal region of the Turnip mosaic virus P3 protein is essential for viral infection via targeting P3 to the viral replication complex. Virology 510, 147–155.
den Boon, J.A., Ahlquist, P., 2010. Organelle-like membrane compartmentalization of positive-strand RNA virus replication factories. Annu. Rev. Microbiol. 64, 241–256.
den Boon, J.A., Diaz, A., Ahlquist, P., 2010. Cytoplasmic viral replication complexes. Cell Host Microbe 8 (1), 77–85.
Diaz, A., Zhang, J., Ollwerther, A., Wang, X., Ahlquist, P., 2015. Host ESCRT proteins are required for bromovirus RNA replication compartment assembly and function. PLoS Pathog. 11 (3), e1004742.
Diaz, A., Wang, X., Ahlquist, P., 2010. Membrane-shaping host reticulon proteins play crucial roles in viral RNA replication compartment formation and function. Proc. Natl. Acad. Sci. U. S. A 107 (37), 16291–16296.
Fujiwara, T., Giesman-Cookmeyer, D., Ding, B., Lommel, S.A., Lucas, W.J., 1993. Cell-to-cell Trafficking of macromolecules through plasmodesmata potentiated by the red clover necrotic mosaic virus movement protein. Plant Cell 5 (12), 1783–1794.
Guseva, S., Milles, S., Jensen, M.R., Salvi, N., Kleman, J.P., Maurin, D., Ruigrok, R.W.H., Blackledge, M., 2020. Measles virus nucleo- and phosphoproteins form liquid-like phase-separated compartments that promote nucleocapsid assembly. Sci. Adv. 6 (14) eaaz7095.
Heinlein, M., Padgett, H.S., Gens, J.S., Pickard, B.G., Casper, S.J., Epel, B.L., Beachy, R. N., 1998. Changing patterns of localization of the tobacco mosaic virus movement protein and replicase to the endoplasmic reticulum and microtubules during infection. Plant Cell 10 (7), 1107–1120.
Heinlein, M., 2015. Plant virus replication and movement. Virology 479–480, 657–671.
Heinrich, B.S., Maliga, Z., Stein, D.A., Hyman, A.A., Whelan, S.P.J., 2018. Phase transitions drive the formation of vesicular stomatitis virus replication compartments. mBio 9 (5) e022290-17.
Hyman, A.A., Weber, C.A., Jülicher, F., 2014. Liquid-liquid phase separation in biology. Annu. Rev. Cell Dev. Biol. 30, 39–58.
Hyodo, K., Hashimoto, K., Kuchitsu, K., Suzuki, N., Okuno, T., 2017. Harnessing host ROS-generating machinery for the robust genome replication of a plant RNA virus. Proc. Natl. Acad. Sci. U. S. A 114 (7), E1282–E1290.
Hyodo, K., Mine, A., Taniguchi, T., Kaido, M., Mise, K., Taniguchi, H., Okuno, T., 2013. ADP ribosylation factor 1 plays an essential role in the replication of a plant. RNA virus 87 (1), 163–176.
Hyodo, K., Okuno, T., 2014. Host factors used by positive-strand RNA plant viruses for genome replication. J. Gen. Plant Pathol. 80, 123–135.
Hyodo, K., Okuno, T., 2016. Pathogenesis mediated by proviral host factors involved in translation and replication of plant positive-strand RNA viruses. Curr. Opin. Virol. 17, 11–18.
Hyodo, K., Okuno, T., 2020. Hijacking of host cellular components as proviral factors by plant-infecting viruses. Adv. Virus Res. 107, 37–86.
Hyodo, K., Suzuki, N., Okuno, T., 2019. Hijacking a host scaffold protein, RACK1, for replication of a plant RNA virus. New Phytol. 221 (2), 935–945.
Hyodo, K., Taniguchi, T., Manabe, Y., Kaido, M., Mise, K., Sugawara, T., Taniguchi, H., Okuno, T., 2015. Phosphatidic acid produced by phospholipase D promotes RNA replication of a plant RNA virus. PLoS Pathog. 11 (5), e1004909.
Ishikawa, K., Miura, C., Maejima, K., Komatsu, K., Hashimoto, M., Tomomitsu, T., Fukuoka, M., Yusa, A., Yamaji, Y., Namba, S., 2015. Nucleocapsid protein from fig mosaic virus forms cytoplasmic agglomerates that are hauled by endoplasmic reticulum streaming. J. Virol. 89 (1), 480–491.
Jiang, Z., Zhang, K., Li, Z., Li, Z., Yang, M., Jin, X., Cao, Q., Wang, X., Yue, N., Li, D., Zhang, Y., 2020. The Barley stripe mosaic virus γb protein promotes viral cell-to-cell movement by enhancing ATPase-mediated assembly of ribonucleoprotein movement complexes. PLoS Pathog. 16 (7), e1008709.
Kaido, M., Abe, K., Mine, A., Hyodo, K., Taniguchi, T., Taniguchi, H., Mise, K., Okuno, T., 2014. GAPDH-A recruits a plant virus movement protein to cortical virus replication complexes to facilitate viral cell-to-cell movement. PLoS Pathog. 10 (11), e1004505.
Kaido, M., Funatsu, N., Tsuno, Y., Mise, K., Okuno, T., 2011. Viral cell-to-cell movement requires formation of cortical punctate structures containing Red clover necrotic mosaic virus movement protein. Virology 413 (2), 205–215.
Kaido, M., Tsuno, Y., Mise, K., Okuno, T., 2009. Endoplasmic reticulum targeting of the Red clover necrotic mosaic virus movement protein is associated with the replication of viral RNA1 but not that of RNA2. Virology 395 (2), 232–242.
Kumar, G., Dasgupta, I., 2021. Variability, functions and interactions of plant virus movement proteins: what do we know so far? Microorganisms 9 (4), 695.
Kusumanegara, K., Mine, A., Hyodo, K., Kaido, M., Mise, K., Okuno, T., 2012. Identification of domains in p27 auxiliary replicase protein essential for its association with the endoplasmic reticulum membranes in Red clover necrotic mosaic virus. Virology 433 (1), 131–141.
Laliberté, J.-F., Sanfaçon, H., 2010. Cellular remodeling during plant virus infection. Annu. Rev. Phytopathol. 48, 69–91.
Laliberté, J.-F., Zheng, H., 2014. Viral manipulation of plant host membranes. Ann. Rev. Virol. 1 (1), 237–259.
Levy, A., Tilsner, J., 2020. Creating contacts between replication and movement at plasmodesmata-A role for membrane contact sites in plant virus infections? Front. Plant Sci. 11, 862.
Levy, A., Zheng, J.Y., Lazarowitz, S.G., 2015. Synaptotagmin SYTA forms ER-plasma membrane junctions that are recruited to plasmodesmata for plant virus movement. Curr. Biol. 25, 2018–2025.
Linnik, O., Liesche, J., Tilsner, J., Oparka, K., 2013. Unraveling the structure of viral replication complexes at super-resolution. Front. Plant Sci. 4, 6.
Liu, J., Blancaflor, E.B., Nelson, R.S., 2005. The tobacco mosaic virus 126-kilodalton protein, a constituent of the virus replication complex, alone or within the complex aligns with and traffics along microfilaments. Plant Phyiol 138 (4), 1853–1865.
Lucas, W.J., 2006. Plant viral movement proteins: agents for cell-to-cell trafficking of viral genomes. Virology 344 (1), 169–184.
Luo, M., Terrell, J.R., Mcmanus, S.A., 2020. Nucleocapsid structure of negative strand RNA virus. Viruses 12 (8), 835.
Meijering, E., Dzyubachyk, O., Smal, I., 2012. Methods for cell and particle tracking. Methods Enzymol. 504, 183–200.
Mine, A., Okuno, T., 2012. Composition of plant virus RNA replicase complexes. Curr. Opin. Virol. 2 (6), 669–675.
Mizumoto, H., Hikichi, Y., Okuno, T., 2002. The 3'-untranslated region of RNA1 as a primary determinant of temperature sensitivity of red clover necrotic mosaic virus Canadian strain. Virology 293 (2), 320–327.
Mizumoto, H., Tatsuta, M., Kaido, M., Mise, K., Okuno, T., 2003. Cap-independent translational enhancement by the 3' untranslated region of red clover necrotic mosaic virus RNA1. J. Virol. 77 (22), 12113–12121.
Monsion, B., Incarbone, M., Hleibieh, K., Poignavent, V., Ghannam, A., Dunoyer, P., Daeffler, L., Tilsner, J., Ritzenthaler, C., 2018. Efficient detection of long dsRNA *in vitro* and *in vivo* using the dsRNA binding domain from FHV B2 protein. Front. Plant Sci. 9, 1–16.
Mori, M., Mise, K., Kobayashi, K., Okuno, T., Furusawa, I., 1991. Infectivity of plasmids containing brome mosaic virus cDNA linked to the cauliflower mosaic virus 35S RNA promoter. J. Gen. Virol. 72, 243–246.
Nagy, P.D., Feng, Z., 2021. Tombusviruses orchestrate the host endomembrane system to create elaborate membranous replication organelles. Curr. Opin. Virol. 48, 30–41.
Nikolic, J., Bars, R.L., Lama, Z., Scrima, N., Lagaudrière-Gesbert, C., Gaudin, Y., Blondel, D., 2017. Negri bodies are viral factories with properties of liquid organelles. Nat. Commun. 8 (1), 58.
Reagan, B.C., Burch-Smith, T.M., 2020. Viruses reveal the secrets of plasmodesmal cell biology. Mol. Plant Microbe Interact. 33 (1), 26–39.
Sambade, A., Brandner, K., Hofmann, C., Seemanpillai, M., Mutterer, J., Heinlein, M., 2008. Transport of TMV movement protein particles associated with the targeting of RNA to plasmodesmata. Traffic 9 (12), 2073–2088.
Schindelin, J., Arganda-Carreras, I., Frise, E., Kaynig, V., Longair, M., Pietzsch, T., Preibisch, S., Rueden, C., Saalfeld, S., Schmid, B., Tinevez, J.Y., White, D.J., Hartenstein, V., Eliceiri, K., Tomancak, P., Cardona, A., 2012. Fiji: an open-source platform for biological-image analysis. Nat. Methods 9 (7), 676–682.
Schoelz, J.E., Leisner, S., 2017. Setting up shop: the formation and function of the viral factories of *Cauliflower mosaic virus*. Front. Plant Sci. 8, 1832.
Schwartz, M., Chen, J., Janda, M., Sullivan, M., den Boon, J., Ahlquist, P., 2002. A positive-strand RNA virus replication complex parallels form and function of retrovirus capsids. Mol. Cell. 9 (3), 505–514.
Schwartz, M., Chen, J., Lee, W., Janda, M., Ahlquist, P., 2004. Alternate, virus-induced membrane rearrangements support positive-strand RNA virus genome replication. Proc. Natl. Acad. Sci. U. S. A 101 (31), 11263–11268.
Szécsi, J., Ding, X.S., Lim, C.O., Bendahmane, M., Cho, M.J., Nelson, R.S., Beachy, R.N., 1999. Development of tobacco mosaic virus infection sites in *Nicotiana benthamiana*. Mol. Plant Microbe Interact. 12, 143–152.
Takeda, A., Tsukuda, M., Mizumoto, H., Okamoto, K., Kaido, M., Mise, K., Okuno, T., 2005. A plant RNA virus suppresses RNA silencing through viral RNA replication. EMBO J. 24 (17), 3147–3157.
Tatsuta, M., Mizumoto, H., Kaido, M., Mise, K., Okuno, T., 2005. The red clover necrotic mosaic virus RNA2 trans-activator is also a cis-acting RNA2 replication element. J. Virol. 79 (2), 978–986.
Tilsner, J., Linnik, O., Louveaux, M., Roberts, I.M., Chapman, S.N., Oparka, K.J., 2013. Replication and trafficking of a plant virus are coupled at the entrances of plasmodesmata. J. Cell Biol. 201 (7), 981–995.
Tilsner, J., Linnik, O., Wright, K.M., Bell, K., Roberts, A.G., Lacomme, C., Cruz, S.S., Oparka, K.J., 2012. The TGB1 movement protein of potato virus X reorganizes actin and endomembranes into the X-body, a viral replication factory. Plant Physiol. 158 (3), 1359–1370.
Tilsner, J., Oparka, K.J., 2012. Missing links? - the connection between replication and movement of plant RNA viruses. Curr. Opin. Virol. 2 (6), 705–711.
Tilsner, J., Taliansky, M.E., Torrance, L., 2014. Plant virus movement. eLS 1–12.
Tremblay, D., Vaewhongs, A.A., Turner, K.A., Sit, T.L., Lommel, S.A., 2005. Cell wall localization of Red clover necrotic mosaic virus movement protein is required for cell-to-cell movement. Virology 333 (1), 10–21.
Turner, K.A., Sit, T.L., Callaway, A.S., Allen, N.S., Lommel, S.A., 2004. Red clover necrotic mosaic virus replication proteins accumulate at the endoplasmic reticulum. Virology 320 (2), 276–290.
Waigmann, E., Ueki, S., Trutnyeva, K., Citovsky, V., 2004. The ins and outs of nondestructive cell-to-cell and systemic movement of plant viruses. Crit. Rev. Plant Sci. 23, 195–250.
Wang, A., 2021. Cell-to-cell movement of plant viruses via plasmodesmata: a current perspective on potyviruses. Curr. Opin. Virol. 48, 10–16.
Wu, X., Cheng, X., 2020. Intercellular movement of plant RNA viruses: targeting replication complexes to the plasmodesma for both accuracy and efficiency. Traffic 21 (12), 725–736.

Xiong, Z., Kim, K.H., Giesman-Cookmeyer, D., Lommel, S.A., 1993a. The roles of the red clover necrotic mosaic virus capsid and cell-to-cell movement proteins in systemic infection. Virology 192 (1), 27–32.
Xiong, Z., Kim, K.H., Kendall, T.L., Lommel, S.A., 1993b. Synthesis of the putative red clover necrotic mosaic virus RNA polymerase by ribosomal frameshifting *in vitro*. Virology 193 (1), 213–221.
Xiong, Z., Lommel, S.A., 1989. The complete nucleotide sequence and genome organization of red clover necrotic mosaic virus RNA-1. Virology 171 (2), 543–554.
Xiong, Z., Lommel, S.A., 1991. Red clover necrotic mosaic virus infectious transcripts synthesized *in vitro*. Virology 182 (1), 388–392.
Yang, X., Li, Y., Wang, A., 2021. Research advances in potyviruses: from the laboratory bench to the field. Annu. Rev. Phytopathol. 59, 1–29.
Zavriev, S.K., Hickey, C.M., Lommel, S.A., 1996. Mapping of the red clover necrotic mosaic virus subgenomic RNA. Virology 216 (2), 407–410.